Particle Accelerators, 1986, Vol. 19, pp. 181–196
0031-2460/86/1904–0181/$20.00/0

Printed in the United States of America

ANALYTICAL AND NUMERICAL STUDIES OF 4-D MAPPING MODELS OF COLLIDING ELECTRON BEAMS

TASSOS BOUNTIS

Department of Mathematics and Computer Science, Clarkson University, Potsdam, NY 13676

(Received March 7, 1985)

Analytical and numerical methods of nonlinear dynamics are applied to some 4-D mapping models of "cylindrical" colliding $e^-(e^+)$ beams, including dissipation and quantum fluctuations. The theory of action-angle variables is used to derive approximate expressions for the location and width of the attracting regions of a major period-4 resonance in the absence of quantum "noise." Numerical experiments demonstrate that damping, by itself, *can enhance* beam blowup near major resonances, and certain so-called fixed distance orbits, by a slow "outward" diffusion process—an effect very similar to that due to noise. Generally, however, damping tends to *reduce* blowup phenomena. Finally, we derive an approximate, but very accurate, *closed-form* expression for the beam–beam force in "elliptic" beam models, thus greatly accelerating the computations by avoiding the numerical evaluation of integrals at every iteration.

I. INTRODUCTION

The problem of stability of colliding particle beams in high-energy accelerators has recently received the attention of several theoretical physicists and applied mathematicians, in view of exciting new developments in the field of nonlinear dynamics.[1–6] It has long been known that the (almost instantaneous) "kicks" experienced by two crossing beams, during the $\sim 10^{11}$ interactions of one high-energy physics experiment, are the result of nonlinear electromagnetic forces which may cause undesirable beam blowup effects and even severe particle loss. However, it has only recently been realized that such beam–beam interaction phenomena can be well described and studied in terms of deterministic systems of difference equations or *mappings* for which several analytical and computational techniques are available.[1–6]

Most of the work so far has concentrated on the conservative case of $p(\bar{p})$ colliding beams, where all radiation-damping effects can be neglected. In this context, several quite successful two- and four-dimensional mapping models were introduced and studied[1–6] using the theory of action-angle variables of Hamiltonian mechanics.[4–7] It is one of the aims of this paper to demonstrate the applicability of action-angle variables to dissipative mapping models of colliding $e^-(e^+)$ beams, for which radiation-damping effects cannot be neglected and are, in fact, expected to play a significant role in beam blowup phenomena caused by the beam–beam interaction.

The second main aim of this paper is to study numerically the effects of adding dissipation and/or quantum fluctuations to the blowup properties of some 4-D mapping models of "cylindrical" colliding beams. What we find is that dissipation, generally, tends to have a blowup-*reducing* effect on the motion. However, for tune ratios close to lowest-order resonances of the model, or for initial conditions near some special solutions of the mapping equations, dissipation actually *enhances* beam blowup, causing a slow "outward" diffusion of the orbits to distances further and further away from the ideal path. Similarly, noise *by itself* appears to always have a blowup-enhancing effect on the motion; however, after dissipation has already been included in the model, noise doesn't seem to significantly affect orbital behavior.

We note that the success of mapping models in simulating the beam–beam interaction of colliding $e^-(e^+)$ beams has been amply demonstrated by the work of Myers and co-workers.[8] We use similar models in our analysis, describing the horizontal (x_t) and vertical (y_t) deflections of a weak beam particle as it collides with a strong, bunched beam according to the difference equations[6]

$$\begin{aligned} x_{t+1} &= -Dx_{t-1} + x_t\left[2C_1 + \frac{BS_1}{Q_1} f(r_t)\right] + E\xi_t, \\ y_{t+1} &= -Dy_{t-1} + y_t\left[2C_2 + \frac{BS_2}{Q_2} f(r_t)\right] + E\eta_t, \end{aligned} \tag{1}$$

where $r_t^2 \equiv x_t^2 + y_t^2$, and $t = 0, 1, 2, \ldots$, counts the beam crossings. Q_1, Q_2 are the horizontal and vertical machine tunes, respectively, $0 \le D \le 1$ is a dissipation parameter, ξ_t, η_t are randomly generated noise variables,

$$C_i \equiv \cos 2\pi Q_i, \qquad S_i \equiv \sin 2\pi Q_i, \qquad i = 1, 2, \tag{2}$$

and B is a measure of the strength of the beam–beam force, related to the "tune-shift" values in the x and y directions, respectively, by $\Delta\nu_i \equiv B/4\pi Q_i$, $i = 1, 2$.

The beam–beam force $f(r_t)$ in Eq. (1) has been derived for cylindrical Gaussian beams to be of the exponential form[9]

$$f(r_t) = f_1(r_t) = 2[1 - \exp(-r_t^2/2)]/r_t^2. \tag{3}$$

However, for reasons of facilitating the derivation of analytical results, we prefer to work here with the alternate expression[6]

$$f(r_t) = f_2(r_t) = 64/(r_t^2 + 8)^2, \tag{4}$$

which yields identical qualitative and very similar quantitative results with Eq. (3). [Note that $f_1(0) = f_2(0)$, $f_1'(0) = f_2'(0)$, $f_1''(0) = f_2''(0)$, and $f_i(r_t) \to 0$ as $r_t \to \infty$.]

Of course, both $f_1(r_t)$ and $f_2(r_t)$ above describe the interaction of beams with *cylindrically* symmetric charge distributions; they are used exclusively for the results of Sections 2 and 3 of this paper. However, in Section 4 we derive for the first time (to our knowledge) a *closed-form* expression for the force in the case of *elliptically* charged beams, which is certainly more appropriate to use when simulating $e^-(e^+)$ colliding-beam experiments.

Our closed-form expressions of Section 4 for elliptic beams have the significant advantage of greatly accelerating computations, by avoiding the numerical evaluation of integrals at every iteration of the mapping. We have not used them in this paper; instead, we prefer to investigate them in future publications, where we shall make a detailed comparison between blowup effects of elliptic beams to those of cylindrical beams. We will then, hopefully, be able to understand better the results of other researchers,[8,10] who have observed some interesting phenomena in their $e^-(e^+)$ mapping models caused by the presence of radiation damping and/or quantum fluctuations.

II. REGIONS OF ATTRACTION OF A 4-D DISSIPATIVE MAP

It is well known that the methods of canonical perturbations and action-angle variables apply and yield very useful results in conservative, Hamiltonian systems and symplectic maps.[1–6] What we shall demonstrate in this section is that they can be extended to apply to *dissipative* mappings as well, where they also yield useful analytical if only approximate results.

Take, for example, the 4-D mapping model, Eq. (1) of the Introduction in the symmetric case $Q_1 = Q_2$ and in the absence of dissipation, i.e., $E = 0$. It is easy to see that it possesses the *t-dependent* integral of the motion

$$x_{t+1}y_t - x_t y_{t+1} = D(x_t y_{t-1} - x_{t-1}y_t) = \cdots = D^t(x_1 y_0 - x_0 y_1). \tag{5}$$

In the conservative case $D = 1$, this is a (t-independent) "angular-momentum" integral, and it can be used to reduce exactly the 4-D model to a 2-D *area-preserving* mapping on the plane.[11]

Note, however, that in the dissipative case $0 < D < 1$ also, as $t \to \infty$, Eq. (5) yields a t-independent integral

$$x_{t+1}/y_{t+1} = x_t/y_t, \qquad \therefore x_t = cy_t, \tag{6}$$

and thus both the x_t and y_t deflections of the weak beam approach (as $t \to \infty$) the solutions of the same 2-D *area-contracting* map

$$z_{t+1} = -Dz_{t-1} + z_t\left[2C + \frac{64BS/Q}{(z_t^2+8)^2}\right], \tag{7}$$

$t = 0, 1, 2, \ldots$, where $C = \cos 2\pi Q$ and $S = \sin 2\pi Q$ as usual, $0 < D < 1$ is the dissipation parameter, and $\Delta\nu = B/4\pi Q$ is the tune shift.

We start our analysis by writing Eq. (7) as a differential equation[12]

$$\ddot{z} = -Q^2 z - R\dot{z} + 64Bz\delta_{2\pi}(t)/(z^2+8)^2, \tag{8}$$

where $(\dot{}) \equiv d(\ )/dt$, $\delta_{2\pi}(t)$ is the 2π-periodic delta function

$$\delta_{2\pi}(t) = \sum_{n=-\infty}^{\infty} \delta(t - 2\pi n) = \frac{1}{2\pi}\sum_{n=-\infty}^{\infty} \cos nt, \tag{9}$$

and $R = -\ln D/2\pi$ is our new dissipation parameter (note $0 < R \ll 1$ near the

conservative limit $D \to 1$). Defining a new dependent variable $Z(t)$ by

$$Z(t) \equiv z(t) \exp(Rt/2), \tag{10}$$

we eliminate the first-derivative term in Eq. (8),

$$\ddot{Z} = -\omega_0^2 Z + 64BZ\delta_{2\pi}(t)/(Z^2 e^{-Rt} + 8)^2,$$

where $\omega_0^2 \equiv Q^2 - R^2/4$, and thus we derive an *exact* Hamiltonian for our system:

$$H = \tfrac{1}{2}(\dot{Z}^2 + \omega_0^2 Z^2) + 32Be^{Rt}\delta_{2\pi}(t)/(Z^2 e^{-Rt} + 8). \tag{11}$$

We now introduce action-angle variables I, ϕ in the usual way:[1-6]

$$Z \equiv (2I/\omega_0)^{1/2} \cos\phi, \qquad \dot{Z} = -(2I\omega_0)^{1/2} \sin\phi, \tag{12}$$

and we rewrite Eq. (11) in the form

$$H = \omega_0 I + \frac{(2B/\pi)e^{Rt}}{A\cos^2\phi + 1}\left(1 + 2\sum_{n=1}^{\infty}\cos nt\right), \qquad A \equiv \frac{Ie^{-Rt}}{4\omega_0}, \tag{13}$$

cf. Eq. (9). Expanding also in Fourier series in ϕ and combining terms we finally rewrite Eq. (13) as

$$H = \omega_0 I + \frac{(4B/\pi)e^{Rt}}{A+2}\left[\sum_{m=0}^{\infty} A_{2m}\cos 2m\phi + \sum_{m=0}^{\infty}\sum_{n=1}^{\infty} A_{2m}\cos(2m\phi - nt)\right], \tag{14}$$

where

$$A_0 = \frac{1}{\sqrt{1-a^2}}; \qquad A_{2m} = \frac{2}{\sqrt{1-a^2}}\left(\frac{\sqrt{1-a^2}-1}{a}\right)^m, \qquad m \neq 0, \tag{15}$$

$a \equiv A/(A+2)$, and use has been made of the formula[13]

$$\int_0^{\infty} \frac{\cos m\theta\, d\theta}{a\cos^2\theta + 1} = \frac{\pi}{\sqrt{1-a^2}}\left(\frac{\sqrt{1-a^2}-1}{a}\right)^m.$$

The time- and angle-*averaged* part of our Hamiltonian Eq. (14) is

$$H_0 = \omega_0 I + \frac{2B}{\pi}e^{Rt}\left(\frac{Ie^{-Rt}}{4\omega_0} + 1\right)^{-1/2}, \tag{16}$$

with the associated frequency

$$\dot{\phi} = \omega = \frac{\partial H_0}{\partial I} = \omega_0 - \frac{\Delta\nu Q}{\omega_0}\left(\frac{Ie^{-Rt}}{4\omega_0} + 1\right)^{-3/2}. \tag{17}$$

Note here that in the neighborhood of an attracting periodic orbit of Eq. (7), where $z_t \to$ constant, $Z(t) \sim \exp(Rt/2)$, cf. Eq. (10); hence $I \sim \exp(Rt)$ and Eq. (17) above gives meaningful results as t increases.

We now select the parameter values $Q = 3.76666$ and $\Delta\nu = 0.02$ and concentrate on the motion *near* the lowest-order resonance of that case,[6] $4\omega - 15 = 0$, i.e., $m = 2$, $n = 15$ in Eq. (14), where the full Hamiltonian may be approximated by

$$H_1 = H_0 + Fe^{Rt}\cos(4\phi - 15t); \; F \equiv 4BA_4/\pi(A+2), \tag{18}$$

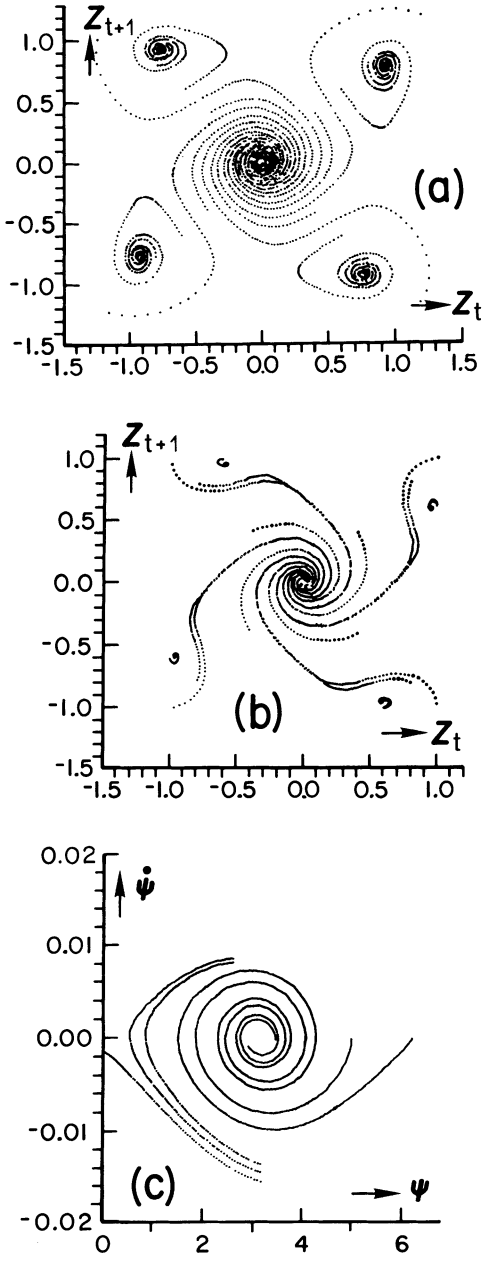

FIGURE 1 (a) Iterates of the dissipative map Eq. (7) on the z_t, z_{t+1} plane at $R = 0.001$. (b) Same as (a) but $R = 0.002$. Note that the stable and unstable 4-resonances are ready to coalesce. (c) Numerical solution of the damped-pendulum Eq. (24) at $R = 0.001$.

cf. Eq. (15) . This resonance, in fact, gives rise to an attracting periodic orbit of the dissipative map (see Fig. 1), whose location in the z_t, z_{t+1} plane is the first thing we shall attempt to approximate using the above formulas.

The action coordinate of this resonance, I_r, can be directly computed from Eq. (17) with $\omega = 15/4$:

$$A_r \equiv \frac{I_r e^{-Rt}}{4\omega_0} = \left[\frac{4\Delta v(1+R^2/8Q^2)}{1/15 - R^2/2Q}\right]^{2/3} - 1, \tag{19}$$

where we have used $\omega_0 \cong Q - R^2/8Q$ for $0 < R \ll 1$. At resonance $\dot{I} = -\partial H/\partial\phi$ must vanish, whence, with $H \cong H_1$, we conclude from Eq. (18) that $\sin 4\phi_r = 0$ at $t = 2\pi n$ and, after some simple analysis,[14]

$$\phi_r = \begin{cases} (2k+1)\pi/4: & \text{stable period-4 orbit} \\ & k = 0, 1, 2, \ldots \\ 2k\pi/4: & \text{unstable period-4 orbit.} \end{cases} \tag{20}$$

Thus the z_t, z_{t+1} coordinates of the stable period-4 resonance, say, can now be estimated by

$$\begin{aligned} z_t = z &= [2Ie^{-Rt}/\omega_0]^{1/2}\frac{\sqrt{2}}{2} = 2\sqrt{A_r}, \\ z_{t+1} &= 2\sqrt{A_r}\exp(-\pi R)(\cos 2\pi\omega_0 - \sin 2\pi\omega_0), \end{aligned} \tag{21}$$

after some algebra using the results of Appendix B in Ref. 12. In Table I, we list the coordinates of the stable period-4 orbit in the first quadrant of the z_t, z_{t+1} plane, as computed exactly by iterating the map Eq. (7) and approximately by Eq. (21).

TABLE I

Coordinates of the stable period-4 orbit in the first quadrant of the z_t, z_{t+1} plane, computed approximately by Eq. (21) and exactly by Eq. (7)

	Approximate		Exact	
R	z_t	z_{t+1}	z_t	z_{t+1}
0.0	0.71901	0.79023	0.86451	0.86451
0.001	0.71901	0.78775	0.92658	0.77075
0.002	0.71903	0.7853	0.94739	0.59738
0.01	0.71943	0.76622	—	—

As expected, the action-angle-variables calculation yields results that are off by 10–20% from the exact coordinates of the period-4 resonance (see also Fig. 1). One useful feature of the approximate results is that they show—in agreement

with the exact results—that the z_t coordinate increases and the z_{t+1} decreases as R grows.

However, an interesting phenomenon occurs already at very small values of R. The stable and unstable period-4 resonances come closer and closer to each other (see Fig. 1b), and at $R \cong 0.0022$ they actually coalesce and disappear, leaving the origin as the only attractor in the z_t, z_{t+1} plane for $R \gtrsim 0.0022$. This coalescence is a fully nonlinear phenomenon not captured by our single-resonance Hamiltonian Eq. (18). Its treatment would require keeping many more of the resonant terms in Eq. (14).

It is important to note that, small as $R \cong 0.0022$ may seem, it corresponds to a dissipation level much higher than one typically expects in practice, i.e., $R \sim 1 \times 10^{-4}$, cf. Ref. 10. Thus, at realistic dissipation rates the period-4 resonance of Eq. (7) will be present, and the action-angle-variable results of this paper should prove to be quite useful.

We now demonstrate the usefulness of our analysis by estimating the size of the region of attraction of this resonance and comparing our results with numerical experiments. To this end, we first derive a *damped-pendulum* equation describing the motion near that resonance. Introducing a new angle variable $\psi \equiv 4\phi - 15t$, differentiating with respect to t, and expanding for $|Ie^{-Rt}/4\omega_0|$ small, yields

$$\dot{\psi} = 4\omega_0 - \frac{4\Delta\nu Q}{\omega_0}\left(1 - \frac{3Ie^{-Rt}}{8\omega_0}\right) - 15, \tag{22}$$

where use has been made of Eq. (17). Differentiating now Eq. (22) once more with respect to t and using it to substitute for $I \exp(-Rt)$ in terms of $\dot{\psi}$ gives

$$\ddot{\psi} = \frac{3Q\Delta\nu}{2\omega_0^2}\dot{I}e^{-Rt} - R\left(\dot{\psi} - 4\omega_0 + \frac{4\Delta\nu Q}{\omega_0} + 15\right). \tag{23}$$

Using, finally, $\dot{I} = -\partial H_1/\partial\phi$ with Eq. (18) and neglecting the small constant term ($\approx 10^{-5}$) in Eq. (23), we arrive at the damped pendulum equation

$$\ddot{\psi} = \frac{6Q\Delta\nu}{\omega_0^2} F \sin\psi - R\dot{\psi}, \tag{24}$$

where F, a, and A in Eqs. (18), (15), and (13) are evaluated at resonance, cf. Eq. (19).

Equation (24) is the analogue of the simple pendulum equation of the conservative ($R = 0$) case first introduced by Chirikov[7] and then used by many others[1-6] in the analysis of nonlinear resonances of $p(\bar{p})$ colliding beams. The exact solution of Eq. (24) is more difficult to obtain than in the $R = 0$ case; however, for the purposes of the approximate theory developed here, it will be sufficient to solve it numerically.

Integrating thus Eq. (24) on the computer for $R = 0.001$ and plotting the solutions on the ψ, $\dot{\psi}$ plane (see Fig. 1c), we find that the orbits are attracted by the resonance as long as $\dot{\psi}(0)$ lies within the range $|\dot{\psi}(0)| \lesssim 0.014$ [with $\psi(0) = \pi$]. Hence, the region of attraction in the z_t, z_{t+1} plane extends approxim-

ately up to where A satisfies

$$4\omega_0 - \frac{4\Delta\nu Q}{\omega_0}(A+1)^{-3/2} - 15 = 0.014. \tag{25}$$

Solving Eq. (25) we find $A = 0.321$, and using it together with $A_r = 0.129$ as computed from Eq. (19), we arrive at an estimate of the *half-width* of the attracting region in the z_t–z_{t+1} plane

$$\Delta z_t = 2(\sqrt{A} - \sqrt{A_r}) = 0.415. \tag{26}$$

Direct comparison with Fig. 1a shows that twice Eq. (26) is in very good agreement with the actual *width* (≈ 0.8) of the attracting region of the period-4 orbit as computed directly by iterating Eq. (7), with $R = -\ln D/2\pi = 0.001$.

III. NUMERICAL EXPERIMENTS, INCLUDING DAMPING AND NOISE

In this section, we return to the general 4-D mapping model of Eq. (1), and include both dissipation and quantum fluctuations

$$\begin{aligned} x_{t+1} &= -Dx_{t-1} + 2x_t\left[C_1 + \frac{BS_1}{Q_1}\frac{1-\exp(-r_t^2/2)}{r_t^2}\right] + E\xi_t, \\ y_{t+1} &= -Dy_{t-1} + 2y_t\left[C_2 + \frac{BS_2}{Q_2}\frac{1-\exp(-r_t^2/2)}{r_t^2}\right] + E\eta_t, \end{aligned} \tag{27}$$

where $r_t^2 = x_t^2 + y_t^2$, $t = 0, 1, 2, \ldots$, and ξ_t, η_t are randomly generated within the interval $(-0.0005, +0.0005)$. The quantity we are interested in computing here is the maximum distance squared of orbit intersections x_t, y_t from the origin, i.e.,

$$p_T^{\max} = \max_{0\le t\le T}(p_t \equiv x_t^2 + y_t^2), \qquad T \gtrsim 10^4. \tag{28}$$

Our main results can be summarized as follows. First of all, a slight amount of damping, of magnitude, say,

$$R \equiv -\ln D/2\pi = 0.00001, \tag{29}$$

can, by itself, enhance beam blowup values of $p_T^{\max}$ to levels higher than those attained when $R = 0$ and $E = 0$ in Eq. (27). How much higher depends on how close the tune ratio $\sigma = Q_2/Q_1$ is to one of the lowest-order resonances of the system, where beam blowup is maximal, with or without dissipation. In σ regions of minimal blowup, damping generally *reduces* $p_T^{\max}$ values. However, even there, in the vicinity of what we call fixed-distance orbits, dissipation often *increases* the value of $p_T^{\max}$ by adding a slow, *diffusive* effect on the motion.

Introducing quantum noise in the conservative map [i.e. setting $E = 1$ with $R = 0$ in Eq. (27)], also significantly increases the values of $p_T^{\max}$ in every case. However, after including dissipation, adding noise to the model does not appear to further enhance blowup in any significant way.

As has been pointed out already in the literature,[6,15] in the conservative case $D = 1$ ($R = 0$) and in the absence of noise ($E = 0$), the mapping, Eq. (27), does not appear to show evident Arnol'd diffusion effects, at least over the first $T = 10^6$–10^7 iterations. This means that over these intervals no slow "leakage" of orbits through higher-order resonances has been observed. It is well known, however, that Arnol'd diffusion is a delicate phenomenon, and its observation requires exceptional care.[7,4]

It is for this reason that, in recent investigations,[6] we have concentrated primarily on the measurement of $p_T^{\max}$ and have plotted it, for several initial conditions, as a function of $\sigma = Q_2/Q_1$. In Fig. 2, we show the results of one such experiment for $x_0 = y_1 = \sqrt{0.1}$, $y_0 = x_1 = 0$.

The first question we would like to ask now is what happens to these results when dissipation and noise effects are taken into account in Eq. (27). To find out, we have performed the same experiment over a range of σ values corresponding to the largest peak of Fig. 2, and we have listed our $p_T^{\max}$ measurements in Table II.

We make two important remarks concerning these results:

(i) First of all, note the blowup-enhancing effect produced by adding noise. It is clearly very evident in the conservative ($R = 0$) case; however, in the presence of dissipation it almost entirely disappears (see 4th column of Table II).

(ii) Generally, dissipation, by itself reduces beam blowup over σ regions where $p_T^{\max}$ is relatively small. However, for $0.925 \lesssim \sigma \lesssim 0.935$, where the largest peak of Fig. 2 lies, dissipation becomes a *blowup-enhancing* effect. In fact, for $\sigma = 0.929$, we found *unbounded* orbits in the 3rd and 4th columns of Table II, where $p_T^{\max} \to \infty$.

It may very well be that the initial conditions used for Fig. 2 and Table II are special. Indeed, the closer one starts near the origin (by taking $p_0, p_1 \lesssim 0.1$), the smaller is the value of $p_T^{\max}$ in the σ regions of minimal blowup, where the origin

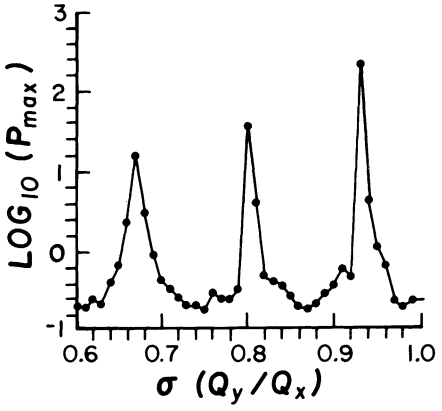

FIGURE 2 $\mathrm{Log}_{10} p_T^{\max}$ vs σ for $\Delta\nu_1 = 0.02$ and $x_0 = y_1 = \sqrt{0.1}$, $y_0 = x_1 = 0$, from Ref. 6. Note maximal blowup near lowest-order resonances at $Q_2 = 5/2$, 3, and 7/2.

TABLE II

Values of $p_T^{\max}$ [cf. Eq. (28)] $\Delta\nu_1 = 0.02$, $Q_1 = 22.6/6$)

	$R = 0.0$: Conservative		$R = 0.00001$: Dissipative	
σ	$E = 0$	$E = 1$	$E = 0$	$E = 1$
0.98	0.23	0.269	0.2284	0.231
0.97	0.283	0.30	0.2811	0.2811
0.96	0.42	0.469	0.4178	0.418
0.95	0.9236	1.03	0.9123	0.92
0.94	4.565	4.585	4.556	4.537
0.936	11.684	14.012	11.662	11.695
0.932	54.286	56.789	55.038	54.978
0.93	452.95	468.89	554.34	545.34
0.928	51.356	52.512	54.194	54.80
0.924	2.6174	2.891	2.6167	2.763
0.92	1.1369	1.138	1.1207	1.1123
0.91	0.4412	0.4549	0.4355	0.4374
0.90	0.2876	0.320	0.2869	0.2866
0.89	0.2178	0.2679	0.209	0.2094
0.88	0.2064	0.2101	0.2052	0.2049
0.87	0.1785	0.1793	0.1762	0.1758

is also (linearly) stable under small perturbations.[6] In these regions, damping appears to have a desirable, *blowup-reducing* effect on the beam.

Near $\sigma = 0.93$, however, initial conditions do not matter much. This is the location of one of the lowest-order resonances of the system,[6] where blowup effects are maximal ($Q_2 = 7/2$). *Resonance "streaming"* phenomena[2] are important in these regions, and their blowup properties are abetted by the presence of dissipation, which now becomes a highly undesirable effect.

Away from major resonances, one might look for minimal beam blowup in the vicinity of what we called *fixed-distance orbits* (f.d.o.'s) of the conservative, undamped 4-D model in Eqs 27:[6] f.d.o.'s are *exact* solutions of the mapping equations, whose distance from the origin is constant ($r_t = r$ for all t) and whose intersections with the x_t, y_t plane rotate by a constant angle $\Delta\theta_t = \Delta\theta$.

Such orbits were found to exist within the "valleys" of Fig. 2 and to be either *stable or unstable,* in the sense that small perturbations in their initial conditions eventually led to small or large deviations away from the exact r, $\Delta\theta$ values of the f.d.o. In Table III, we list some typical f.d.o.'s together with their stability properties for $R = 0$, $E = 0$.

Interestingly enough, the *rates* (in t) at which the "final" values in the $p_T^{\max}$ column of Table III are attained are not the same for all σ. In fact, for both $\Delta\nu_1$ time shifts, when the σ value was closest to the high resonance peaks of Fig. 2, the *"diffusion"* of the orbits to larger and larger distances from the origin (i.e., the *growth* of p_t from p_0 to $p_T^{\max}$) became more and more steady and continuous. On the other hand, at other σ values, $p_T^{\max}$ was attained rather quickly (after, say, 3000 iterations) and appeared to remain unchanged thereafter even for $T \gtrsim 10{,}000$.

TABLE III

Typical F.d.o.'s, with stability properties, for $R = 0$, $E = 0 (Q_1 = 22.6/6)$

σ	$\Delta\nu_1 = 0.02$		$\Delta\nu_1 = 0.106$		$P_T^{\max}$ after a small perturbation of p_0
	$p = r^2$	$\cos \Delta\theta$	$p = r^2$	$\cos \Delta\theta$	
0.9			1.08625	−0.40655	1.0863 (stable)
0.89			2.61212	−0.26524	2.6172 (stable)
0.88			4.98333	−0.1393	51.06 (unstable)
0.868	0.70284	-8.488×10^{-4}			0.7185 (stable)
0.865	2.44607	0.032420			16.167 (unstable)
0.6	3.1770	0.041922			20.35 (unstable)

The type of "diffusion" phenomenon in the vicinity of *stable* f.d.o.'s was actually found to be *enhanced* when dissipation and noise were added to the model. In Table IV we list the results of some typical numerical experiments of beam blowup *near* f.d.o.'s.

Whether this orbital diffusion we have observed (with or without dissipation) is due to resonance "streaming"[2] or to actual Arnol'd diffusion remains still an open question. We are currently pursuing this investigation further, analytically and numerically, to gain a better understanding of these interesting blowup phenomena. One of the questions, for example, is: to what extent can the motion near our unstable and stable f.d.o.'s be attributed to what some authors have called "thick-layer" and "thin-layer" diffusion, respectively,[16,4] in the iteration of 4-D maps?

Having thus improved our understanding of diffusion in the cylindrical-beam case, we intend to turn our attention to the elliptically symmetric beam–beam interaction, for which we derive an approximate potential in Section 4. New parameters enter there, like the "aspect ratio" b/a of the strong beam, whose variation may yield different blowup properties in the x (or the y) direction. These phenomena are currently being studied, and results will appear in future publications.

TABLE IV

Values of $p_T^{\max}$

	$\Delta\nu_1 = 0.02$			$\Delta\nu_1 = 0.106$		
	$E = 0$		$E = 1$	$E = 0$		$E = 1$
σ	$R = 0$	$R = 0.00001$		$R = 0$	$R = 0.00001$	
0.9				1.0863	1.171	1.222
0.89				2.6172	2.686	2.843
0.88				51.06	49.393	49.96
0.868	0.7185	0.7984	0.7827			
0.865	16.17	15.05	14.76			
0.6	20.35	19.23	19.26			

IV. CLOSED-FORM EXPRESSIONS FOR THE INTERACTION POTENTIAL IN ELLIPTIC BEAMS

All the results of this paper and those of our earlier publications[6,11] have been restricted to the case of beams, whose charge distribution is *cylindrically symmetric* in the x and y directions, i.e., where the potential of the beam–beam interaction,[9]

$$V_E(x, y) = \int_0^\infty \frac{1 - \exp\left[-x^2/(a^2+s) - y^2/(b^2+s)\right]}{(a^2+s)^{1/2}(b^2+s)^{1/2}}\, ds. \tag{30}$$

is to be obtained from a cylindrical bi-Gaussian with $a = b$. In that case, the integral Eq. (30) becomes an error function, and its partial derivatives yield the beam–beam force in the x, y directions in *closed form*:

$$\frac{1}{x}\frac{\partial V_E}{\partial x} = \frac{1}{y}\frac{\partial V_E}{\partial y} = \frac{1 - \exp\left[-(x^2+y^2)/2\right]}{(x^2+y^2)/2}, \tag{31}$$

with $a = b = \sqrt{2}$, cf. Eq. (1) with Eq. (3). Such closed-form expressions, however, are not available for the *elliptic beam* case $a \neq b$, for which the integral Eq. (30)—or its x, y partial derivatives—appears impossible to evaluate analytically.

The absence of analytical results for the interaction force between elliptic beams has so far compelled researchers either to resort to "flat-beam" ($b \ll a$) approximations or to numerically compute integrals of the form of Eq. (30) at *every iteration* of the mapping equations—a very time-consuming task (if one wants to perform many iterations), even for the fastest computers available today. The best that has been achieved so far—at least to the knowledge of this author—in terms of speed in such calculations is in recent work of S. Myers and his group at CERN,[8] who use efficient interpolation schemes with tables of complex error functions.

In this section, we derive *closed-form* analytical expressions, which are excellent approximations of the interaction potential Eq. (30) for a $a \neq b$. We believe our results are important not only for $e^-(e^+)$ colliding beams, where the beams necessarily become elliptic by unsymmetric blowup in x and y[17] but also in $p(\bar{p})$ experiments, whenever ellipticity effects become unavoidable or perhaps even desirable.

We start our analysis by observing that the beam–beam force given by the exponential function, Eq. (3), gives in the $a = b$ case results very similar to those of the rational function, Eq. (4). This latter function is derived (by x, y partial differentiation) from the potential

$$V_R(x, y) = \int_0^\infty \frac{x^2/(a^2+s) + y^2/(b^2+s)}{\left[1 + x^2/4(a^2+s) + y^2/4(b^2+s)\right]^2} \cdot \frac{ds}{(a^2+s)^{1/2}(b^2+s)^{1/2}} \tag{32}$$

for $a = b = \sqrt{2}$, cf. Eq. (31). Unfortunately, this integral does not appear possible to evaluate analytically either, in the general case $a \neq b$. As we shall see below, however, it lends itself, much more easily than Eq. (30), to analytical approximations which turn out to yield remarkably accurate results.

After some elementary manipulations, we rewrite Eq. (32) in the more convenient form

$$V_R(x, y) = 4\int_0^\infty \frac{(As + B)(s^2 + Cs + D)^{1/2}\, ds}{[s^2 + s(C + A) + B + D]^2}, \tag{33}$$

where

$$A \equiv (x^2 + y^2)/4, \qquad B \equiv (b^2x^2 + y^2a^2)/4, \qquad C \equiv a^2 + b^2, \qquad D \equiv a^2b^2, \tag{33a}$$

and, setting $b \equiv a(1 - \varepsilon)$, we expand the expression

$$[s^2 + Cs + D]^{1/2} = a^2\left\{S - \frac{\Delta}{2S} - \frac{\Delta^2}{8S^3} - \frac{\Delta^3}{16S^5} - \cdots\right\}, \tag{34}$$

with

$$\Delta \equiv \left(\varepsilon - \frac{\varepsilon^2}{2}\right)^2, \qquad S \equiv \frac{1}{a^2}\left(s + \frac{a^2 + b^2}{2}\right). \tag{34a}$$

Before using Eq. (34) in Eq. (33) to derive our closed-form expressions, it is instructive to examine, at this stage, the accuracy of the approximation, Eq. (34), in the evaluation of Eq. (33) and also the accuracy of Eq. (33) *itself* as an approximation of the more commonly used exponential form of the potential $V_E(x, y)$ of Eq. (30).

Some typical results of these comparisons are shown in Fig. 3. Computing numerically $V_E(x, y)$ as given by Eq. (30) for $a = 1$ and $b = 0.5$, and $V_R(x, y)$ as given by Eq. (33), we find very good agreement over large ranges of x, y around the center of the beam. The approximation of Eq. (33) by an integral involving terms up to order Δ in Eq. (34) is found to be virtually indistinguishable from the "exact" Eq. (33)—to the resolution of this graph—at least for $1 \geq b \gtrsim 0.5$. For smaller values of b, we found that it is necessary to keep also the terms of order Δ^2 (and perhaps even Δ^3) in Eq. (34) to achieve an equally high degree of accuracy.

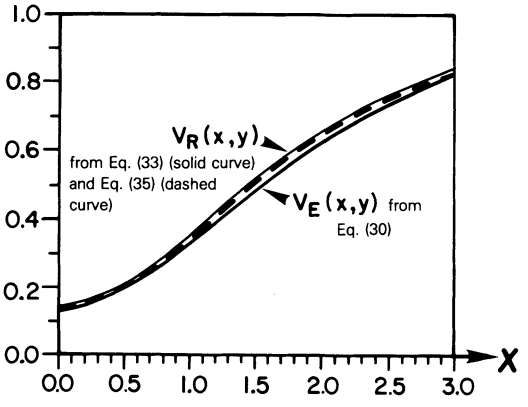

FIGURE 3 Comparison between the exponential and rational potentials of the elliptic beam–beam force at $a = 1.0$, $b = 0.5$, and $y = 0.5$.

We now demonstrate how one can obtain closed-form expressions for Eq. (33), as functions of x, y, which can be differentiated with respect to x and y and then implemented directly in the numerical iterations of the mapping equations, at least for $a > b \gtrsim a/2$. Substituting Eq. (34) up to terms of order Δ in Eq. (33), we find that we must perform the following integrations:

$$\tfrac{1}{4}V_R = A\int_0^\infty \frac{s^2\,ds}{Q(s)} + \left(\frac{AC}{2}+B\right)\int_0^\infty \frac{s\,ds}{Q(s)} + \frac{BC}{2}\int_0^\infty \frac{ds}{Q(s)}$$
$$-\frac{a^4\Delta}{2}\int_0^\infty \frac{ds(As+B)}{(s+C/2)Q(s)}; \qquad Q(s)\equiv[s^2+s(C+A)+B+D]^2. \quad (35)$$

All we need for the evaluation of the above integrals is the result[13]

$$I=\int_0^\infty \frac{ds}{s^2+2\beta s+\gamma} = \frac{1}{2\sqrt{\beta^2-\gamma}}\ln\left[\frac{\beta+\sqrt{\beta^2-\gamma}}{\beta-\sqrt{\beta^2-\gamma}}\right], \quad (36)$$

(for $\beta^2 > \gamma$, which is true in our case). Defining

$$2\beta \equiv C+A, \qquad \gamma \equiv B+D, \qquad \alpha \equiv B/A, \qquad \delta \equiv C/2, \quad (37)$$

we observe that $\int_0^\infty ds/Q(s) = -\partial I/\partial\gamma$ and that the remaining integrals in Eq. (35) can be evaluated directly from the above results by elementary manipulations like partial fraction decompositions, etc. The final result is:

$$V_R = \frac{I}{\beta^2-\gamma}[-A(B+2D-C\beta)-\beta\mathscr{E}+\mathscr{F}] - 2I(\beta\mathscr{A}-\mathscr{D})$$
$$+\frac{1}{\beta^2-\gamma}\left[A^2+\frac{\beta}{\gamma}(BC-\mathscr{F})-2B+\mathscr{E}\right]+2\mathscr{A}\ln\frac{\delta}{\sqrt{\gamma}}, \quad (38)$$

where

$$\mathscr{A} \equiv a^4\Delta A(\alpha-\delta)/(\delta^2-2\beta\delta+\gamma)^2, \qquad \mathscr{D} \equiv (2\beta-\delta)\mathscr{A}, \quad (39a)$$
$$\mathscr{E} \equiv -\mathscr{A}(\delta^2-2\beta\delta+\gamma), \qquad \mathscr{F} \equiv a^4\Delta A + (2\beta-\delta)\mathscr{E}. \quad (39b)$$

We have used the above formulas directly and have also computed numerically the integral Eq. (33) of the rational potential for different values of b and different ranges of x and y. Some typical results are shown here in Fig. 4 for $a = 1$ and $b = 0.8$ and 0.5. The accuracy of the first-order formulas, Eqs (38) and (39), is surprisingly good, as it is not even possible to distinguish between the two results at the resolution of these figures.

For $b < a/2$ one needs to keep more terms in the expansion Eq. (34). We checked numerically that this indeed improves significantly the accuracy of the approximations. The calculations, of course, become more complicated, but the integrals are all analytically tractable. Furthermore, allowing for synchrotron oscillations (and charge variation) *along* the direction of the beam would lead to a *tri-Gaussian* potential Eq. (30), and a corresponding modification of our rational potential Eq. (32). We believe that similar approximations of the type we described in this section can also be made in that case to yield closed-form expressions for the beam–beam force.

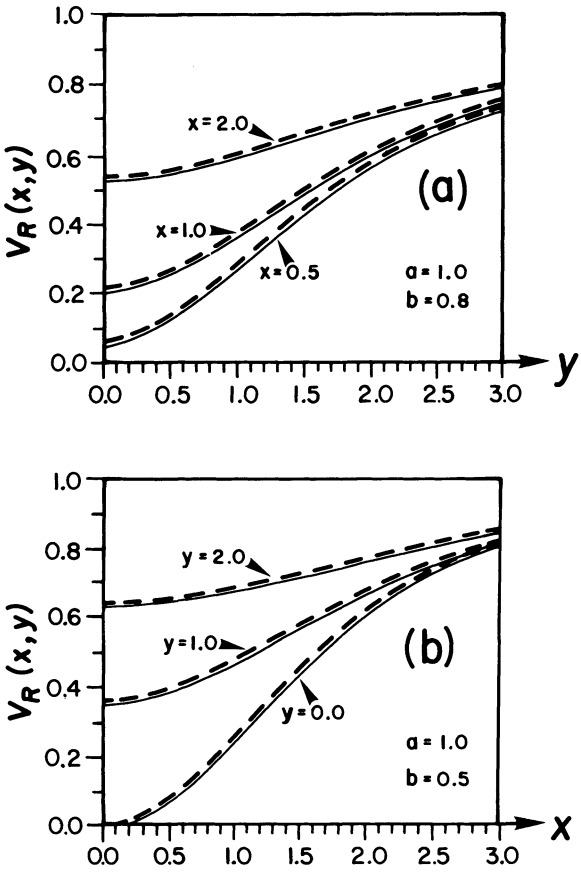

FIGURE 4 Comparison between numerical [Eq. (33), solid curve] and analytical [Eq. (35), dashed curve] calculation of the potential $V_R(x, y)$. Note that, to this resolution, the two curves are indistinguishable.

We are currently in the process of performing these calculations, and results will appear in future publications.[18] The road has been cleared for a full and thorough *numerical* study of the elliptic-beam case. As the complications of the above formulas, however, indicate, it will be some time before any progress is made theoretically using, e.g., resonance analysis as in Section 2, or otherwise.

V. ACKNOWLEDGMENTS

The author wishes to thank the Department of Energy and Drs. David Sutter and Richard Sah for supporting part of this research under Contract DE-FG02-84ER40144. Some of the computations described here were done by M. Bier and V. Papageorgiou, with whom the author also acknowledges many useful discussions on the results of this paper.

REFERENCES

1. J. C. Herrera, in *Nonlinear Dynamics and the Beam–Beam Interaction,* edited by M. Month, AIP Conf. Proc. **57** (A.I.P., New York, 1979).
2. J. Tennyson, in *Physics of High Energy Accelerators,* Fermilab Summer School, 1981 Proceedings, edited by R. A. Corrigan, F. R. Huson, and M. Month, AIP Conf. Proc. **87** (A.I.P., New York, 1982).
3. *Topics in Nonlinear Dynamics,* edited by S. Jorna, AIP Conf. Proc. **46** (A.I.P., New York, 1978).
4. M. Lieberman and A. Lichtenberg, *Regular and Stochastic Motion,* Appl. Math. Series (Springer, 1983).
5. *Long-Time Prediction in Dynamics,* edited by C. Horton, L. Reichl, and V. Szebehely (Wiley Interscience, New York, 1983).
6. T. Bountis, N. Budinsky, and C. R. Eminhizer, *Nucl. Instr. Meth.,* **227** 205 (1984).
7. B. V. Chirikov, *Phys. Rep.,* **52** 265 (1979).
8. S. Myers, CERN Report CERN-ISR-RF/81-08; see CERN Report CERN-ISR/RF/82-06 submitted to Nucl. Instr. Meth; also LEP Notes 188, 310, 327, and 501.
9. See, e.g., the article in J. C. Herrera in Ref. 1.
10. J. Tennyson, SLAC Publ. 2624, Conf. 8005102 (1980).
11. T. Bountis, C. R. Eminhizer, and R. H. G. Helleman, in *Long-Time Predictions in Dynamics,* edited by C. Horton, L. Reichl, and V. Szebehely (Wiley Interscience, New York, 1983).
12. R. H. G. Helleman, in *Long-Time Predictions in Dynamics,* edited by C. Horton, L. Reichl, and V. Szebehely (Wiley Interscience, New York, 1983).
13. I. S. Gradshteyn and I. M. Ryzhik, *Tables of Integrals, Series and Products* (Academic Press, New York, 1965).
14. G. H. Walker and J. Ford, *Phys. Rev.,* **188** 416 (1969).
15. D. Neuffer, A. Riddiford, and A. Ruggiero, Fermilab Report FN-333, FN-343, and FN-346 (1981).
16. J. L. Tennyson, M. Lieberman, and A. Lichtenberg, in *Nonlinear Dynamics and the Beam–Beam Interaction,* edited by M. Month, AIP Conf. Proc. **57** (AIP)., New York, 1979).
17. H. Wiedemann, SLAC Publ. 2624, Conf. 8005102 (1980).
18. T. Bountis, M. Bier, and V. Papageorgiou, *Orbital Diffusion Effects in Mapping Models of Colliding Elliptic Beams,* in preparation.